Dynamic modeling of injection-induced fault reactivation and ground motion and impact on surface structures and human perception

J. Rutqvist, F. Cappa, A. Rinaldi, M. Godano

Available online at www.sciencedirect.com

ScienceDirect

Energy Procedia 63 (2014) 3379 – 3389

Energy Procedia

GHGT-12

Dynamic modeling of injection-induced fault reactivation and ground motion and impact on surface structures and human perception

Jonny Rutqvist[a,] *, Frederic Cappa[a,b], Antonio P. Rinaldi[a], Maxime Godano[b]

[a]*Lawrence Berkeley National Laboratory, Earth Sciences Division, Berkeley, CA 94720, USA*
[b]*GeoAzur, University of Nice Sophia-Antipolis, C´ote d'Azur Observatory, 06560, Sophia-Antipolis, Franc*

Abstract

We summarize recent modeling studies of injection-induced fault reactivation, seismicity, and its potential impact on surface structures and nuisance to the local human population. We used coupled multiphase fluid flow and geomechanical numerical modeling, dynamic wave propagation modeling, seismology theories, and empirical vibration criteria from mining and construction industries. We first simulated injection-induced fault reactivation, including dynamic fault slip, seismic source, wave propagation, and ground vibrations. From co-seismic average shear displacement and rupture area, we determined the moment magnitude to about $M_w = 3$ for an injection-induced fault reactivation at a depth of about 1000 m. We then analyzed the ground vibration results in terms of peak ground acceleration (PGA), peak ground velocity (PGV), and frequency content, with comparison to the U.S. Bureau of Mines' vibration criteria for cosmetic damage to buildings, as well as human-perception vibration limits. For the considered synthetic $M_w = 3$ event, our analysis showed that the short duration, high frequency ground motion may not cause any significant damage to surface structures, and would not cause, in this particular case, upward CO_2 leakage, but would certainly be felt by the local population.

Peer-review under responsibility of the Organizing Committee of GHGT-12

Keywords: Induced seismicity; modeling; carbon sequestration; fault reactivation; ground vibration; building damage; human perception

* Corresponding author. Tel.: +1-510-486-5432; fax: +1-510-486-5686.
E-mail address: JRutqvist@lbl.gov

Peer-review under responsibility of the Organizing Committee of GHGT-12
doi:10.1016/j.egypro.2014.11.367

1. Introduction

The potential of injection-induced fault reactivation associated geologic carbon sequestration, an issue long recognized in the research community [1, 2, 3], has now received increased attention among CO_2 sequestration stakeholders and media as an issue of concern, especially after two recent high-profile publications [4, 5]. Concerns are related to the potential for triggering notable (felt) seismic events and how such events could impact the long-term integrity of a Geologic CO_2 repository [4, 5, 6]. For example, Zoback and Gorelick [5] concluded that there is a high probability that earthquakes would be triggered by injection of large volumes of CO_2 into the brittle rocks commonly found in continental interiors, and because even small- to moderate-sized earthquakes threaten the seal integrity of CO_2 repositories, large-scale carbon capture and storage would be a risky and likely unsuccessful strategy for significantly reducing greenhouse gas emissions to the atmosphere.

In this paper we summarize recent dynamic model simulations of injection-induced fault reactivation, seismicity and its potential impact on surface structures and nuisance to the local human population [7]. It is an integrated analysis from cause to consequence, including the whole chain of processes, from earthquake inception in the subsurface, wave propagation towards the ground surface, and to assess the consequences of ground vibration (Fig. 1). We used coupled multiphase fluid flow and geomechanical numerical modeling, dynamic wave propagation modeling, seismology theories, and empirical vibration criteria from mining and construction industries to present a more quantitative view on induced seismicity associated with geologic carbon sequestration.

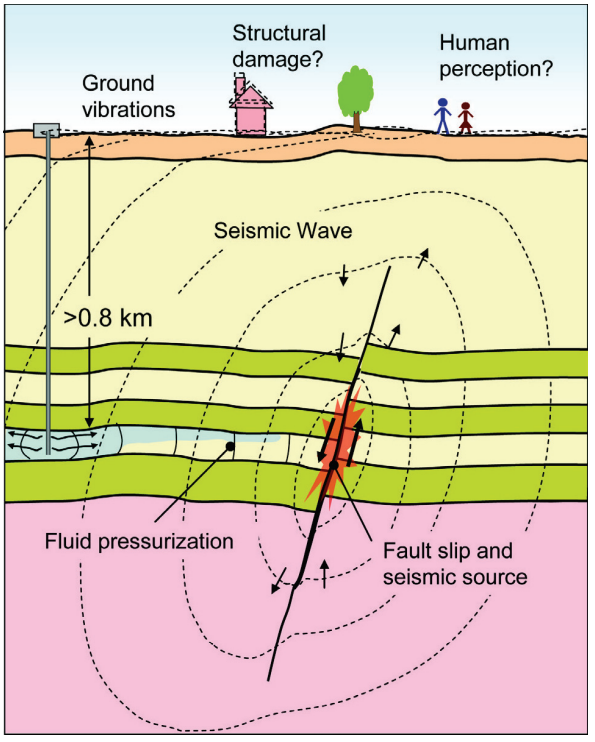

Fig. 1. Schematic of injection-induced fault reactivation, wave propagation, and ground motions, and potential impact on surface structures and human perception [7]..

2. Modeling approach and setup

The simulations summarized in this paper were conducted with the coupled thermo-hydro-mechanical code TOUGH-FLAC [8], which has previously been applied to model fluid-induced fault reactivation, in both generic and site specific studies [9 – 19]. The TOUGH-FLAC code is based on linking the TOUGH2 finite-volume simulator for multiphase fluid flow [20], and the FLAC^{3D} finite-difference code geomechanics and dynamic wave propagation [21]. The approach adopted here involves coupled fluid flow and geomechanical numerical modeling to simulate CO_2 injection and fault rupture. Then, seismological theories are used to calculate the seismic source parameters. A strain-softening fault constitutive model enables modeling of sudden, dynamic fault rupture, and provides a source for wave-propagation and ground-motion calculations [13]. The wave-propagation was calculated using the FLAC^{3D} dynamic analysis option based on an explicit finite difference scheme to solve the full equations of motion in a fully nonlinear analysis (see [21] for details).

The model problem involves a reservoir bounding fault with a dip angle of 80°, width of 2.5 m, and tectonic shear displacement offset (throw) of 125 m (Fig. 2). The models simulations were conducted in a vertical cross section normal to the strike of the fault represented in a 2D plane-strain model (2 km × 2 km). The storage formation is 100 m thick and bounded at the top and bottom by low-permeability 150 m thick formations, which, in turn, is surrounded by two other permeable formations. Similar model geometry has been applied in several of the aforementioned studies of different aspects of injection-induced fault activation.

Initial conditions for the model simulations were derived assuming (1) hydrostatic fluid pressure with the ground water table adjacent to the ground surface, (2) a temperature assuming a depth gradient of 25°C/km with a ground-surface temperature of 10°C, and (3) a vertical stress from the weight of the overburden rock for a bulk density of density $\rho = 2260$ kg/m^3, with the initial minimum horizontal stress being scaled by a factor 0.7 of the vertical stress, i.e. $\sigma_h = 0.7\sigma_v$. The minimum horizontal stress is assumed to be oriented normal to the strike of the fault plane, whereas the maximum horizontal stress is assumed to be oriented parallel to the strike of the fault plane. With these parameters, the initial fluid pressure and temperature at the depth of the CO_2 injection zone (1000 m) is about 10 MPa and 35°C, respectively, whereas the vertical stress is 22.2 MPa and minimum horizontal stress is 15.5 MPa.

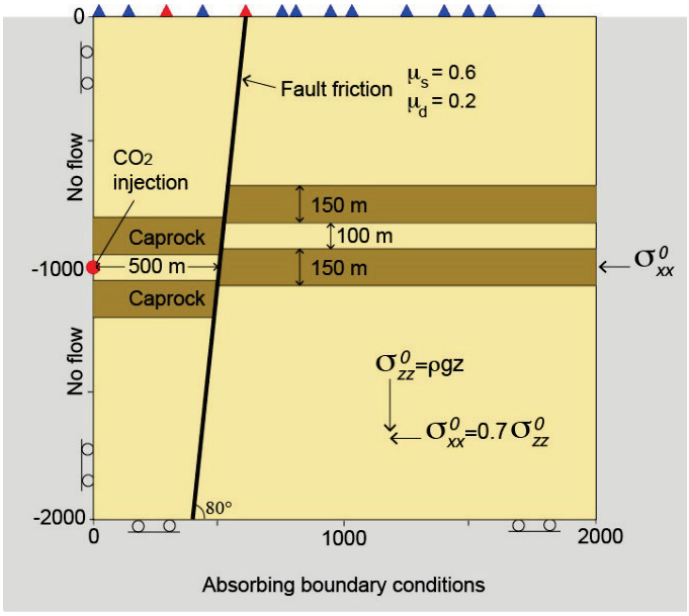

Fig. 2. Model geometry and boundary conditions and ground-motion recording stations (blue and red triangles) [7].

In the model simulations, CO_2 was injected as a point source within the storage formation, with a constant rate of 0.02 kg/m/s (i.e. 630.72 tons/m/year). The simulations were conducted to intentionally induce fault reactivation, which occurred at a high reservoir pressure in a stress regime that favors reactivation of the steeply dipping fault. To reactivate the fault, we had to increase the injection pressure to exceed the initial minimum principal stress (about 7 MPa overpressure).

Properties for the permeable formations and the bounding low-permeable layers represent sandstone and shale, respectively. The fault is modeled using an elasto-plastic anisotropic Mohr-Coulomb model, a built-in FLAC^{3D} constitutive model [21]. The strain-softening fault geomechanical behavior was achieved by a reduction of the coefficient of friction during co-seismic shear slip from a peak static value, $\mu_s = 0.6$, to a dynamic value, $\mu_d = 0.2$, over a critical plastic strain of 10^{-3} [13]. Other properties are defined in [7] and include Young's modulus of 10 GPa for all formations, except for the fault zone, which has a Young's modulus of 5 GPa. The permeability of the injection zone, caprock, and fault is respectively 10^{-13}, 10^{-19}, and 10^{-16} m^2. The values taken for the input parameters of the fault are discussed and justified in Rutqvist et al. [7], though we recognize that these are uncertain, and we consider the selected parameters in this analysis as one set of possible parameters designed for generating a reasonable injection-induced seismic event for our study.

3. Fault reactivation and wave propagation

Fig. 3 presents a set of results related to the reactivation of the fault. For the assumed system and injection rate, the simulation showed that after about 40 days of injection, a dynamic fault rupture nucleates at the base of the CO_2 reservoir. At the initiation of the fault rupture, the fluid pressure had increased by about 7.5 MPa, i.e., achieving a total fluid pressure of 17.5 MPa, a few MPa higher than the local initial minimum principal stress at 1000 m depth. Moreover, as shown in Fig. 3b, the increasing reservoir pressure cause a simultaneous increase in shear stress and reduction of effective normal stress, until the stress state reach the $\mu_s \cdot \sigma$ failure surface (quasi-static model phase in Fig. 3b). After the stress-state reaches the $\mu_s \cdot \sigma$ failure surface, the fault reactivates with a sudden shear stress drop of about 1.4 MPa, as the friction drops to residual value and the shear stress equilibrates with the residual shear strength (dynamic phase in Fig. 3b). The fault reactivation induces localized plastic shear strain distributed over a length of about 290 m, with a maximum shear strain in a portion of the fault just below the reservoir (red zone in Fig. 3a). Based on the calculated co-seismic fault rupture length and average shear-slip displacement (290 m and 0.03 m), we quantified the overall size of the seismic event using seismology relationships by Hanks and Kanamori [22], and Kanamori and Anderson [23]. A seismic moment, $M_0 = 3.48 \times 10^{13}$ Nm and a moment magnitude in the range of $M_w \approx$ 2.5 to 3 were calculated [7].

The simulated sudden fault rupture generated seismic waves that propagated and hit the ground surface at the speed corresponding to the P and S wave velocities for the medium of respectively Cp = 2360 m/s and Cs =1402 m/s. In the simulation wave attenuates by geometric spreading, pore fluid interaction, scattering, and by a substantial dissipation associated with plastic flow in the fault. The model simulation of ground motion was verified using the simulated ground-motion wave train in an inverse analysis to estimate source parameters (moment magnitude, rupture dimensions and stress drop), achieving good agreement and thereby verifying the modeling of the chain of processes from earthquake inception to ground vibration [7].

4. Ground motion accelerations and velocities

Fig. 4 and 5 present acceleration and velocity footprints recorded at 14 assumed stations along the ground surface (red and blue triangles in Fig. 1), for a complete picture of the ground motion and how it is distributed. Fig. 4 shows that the highest values of acceleration are along the horizontal component and are concentrated around the fault (Fig. 4a at x ≈ 675 m), whereas the acceleration values quickly attenuate away from the fault. In general the results in Fig. 4 show a peak ground acceleration (PGA) less than 0.1 g, except for the horizontal component near the fault, where the PGA is 0.6 g. Fig. 5 shows that the highest velocities are also associated with horizontal ground motion around the fault, with a maximum peak ground velocity (PGV) of about 30 mm/s (Fig. 5a at x = 675 m). As with PGA, the PGV magnitude also decreases for stations away from the fault being in the range of 2 to 10 mm/s, with the lowest values at the most distant stations.

Fig. 6 shows a close up of the ground motion response where the fault intersects the ground surface and the highest values of PGA and PGV where obtained. In this figure we also included modeling results with and without a softer soil layer near the ground surface to investigate potential damping or amplification of such a superficial layer. In this layer we assumed a modulus half of that of the bedrock, with a thickness of 50 and 100 m. Fig. 6a shows that the high frequency accelerations are substantially damped in the case of a 50 or 100 m thick superficial soil layer (compare red and blue curves, in Fig. 6a). Still high acceleration continues for several seconds. Fig 6b shows that the maximum PGV is associated with one main jolt having a period of about 0.1 to 0.2 seconds, i.e., a frequency of about 5 to 10 Hz. This main jolt is followed by smaller velocity peaks at somewhat higher frequencies. The soil layers have little effect on the main velocity jolt, with some slight amplification in the case of thicker soil, whereas the subsequent higher frequency velocity peaks are substantially damped in the case of thicker soil. As discussed in Rutqvist et al., [7], the ground motion results obtained in this simulation are reasonable and consistent with field observations of shallow seismicity. This includes the PGA and PGV values and frequencies, which are consistent with field monitoring for same depth range and magnitude [24–26], as well as the phenomenon of high acceleration around faults [27, 28], which in this case is also affected by directivity effects. i.e., focusing or piling up of wave energy in the direction of rupture [7].

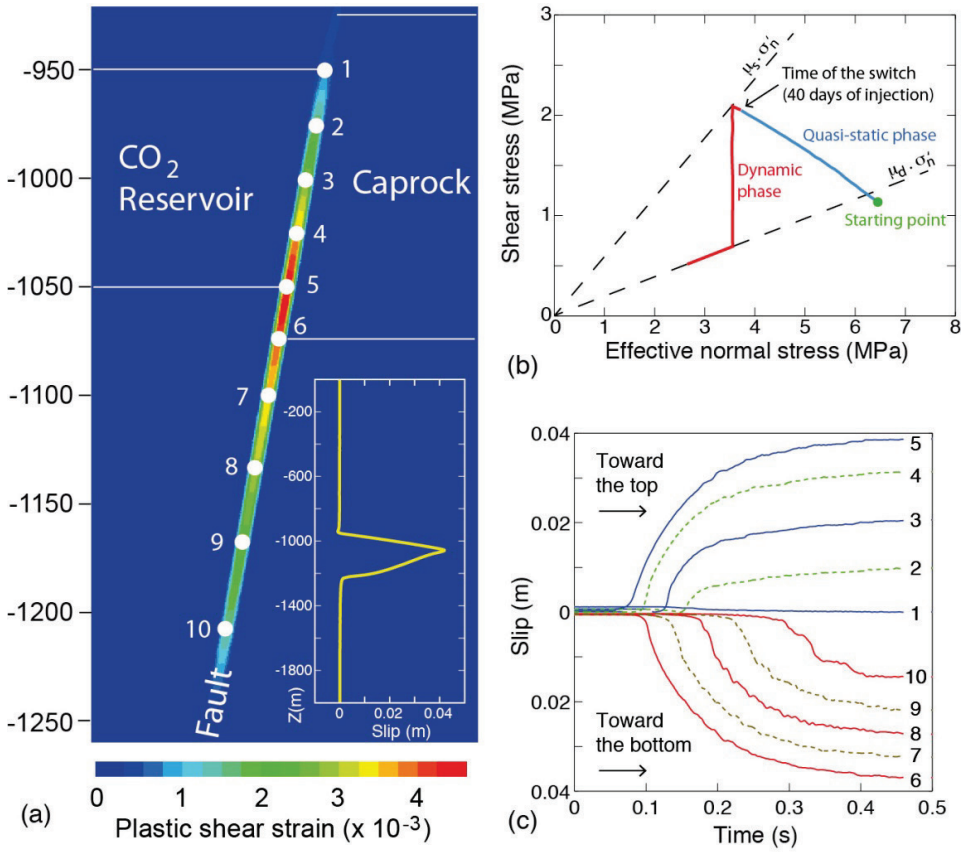

Fig. 3. Simulations results after [13]: (a) Plastic shear strain in the ruptured area and slip profile at the time of seismic rupture (white dots are control points), (b) shear stress-versus-effective normal stress path in the nucleation zone (control point 5 in (a)) of the rupture within the fault (the slow quasi-static phase is in blue and the dynamic phase is in red), (c) slip as function of time at different control points along the fault (white dots in (a)).

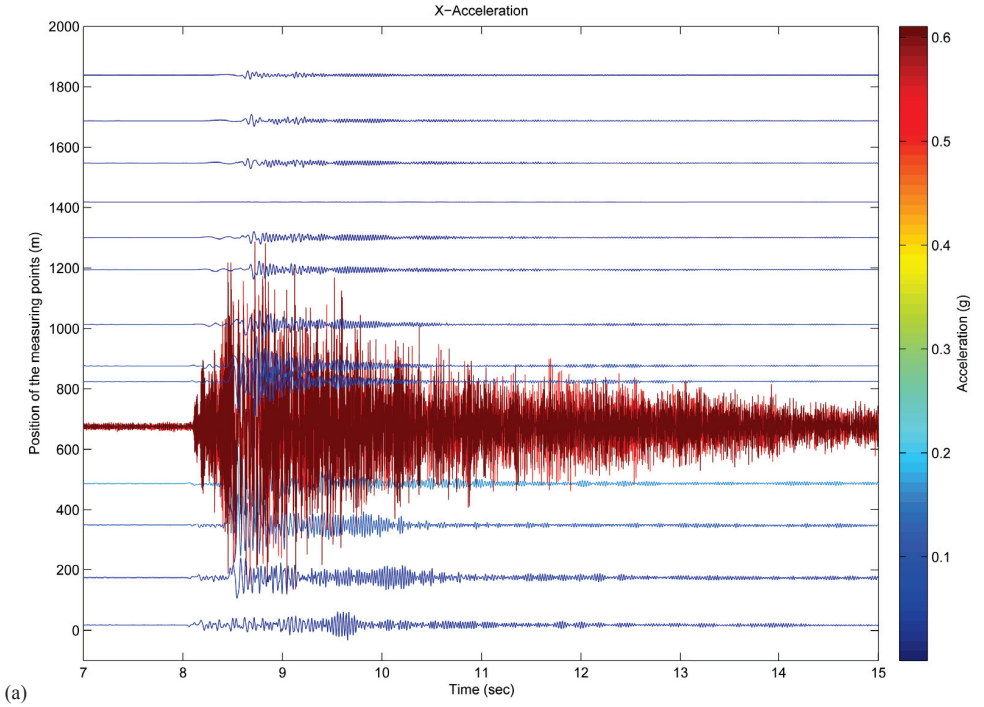

(a)

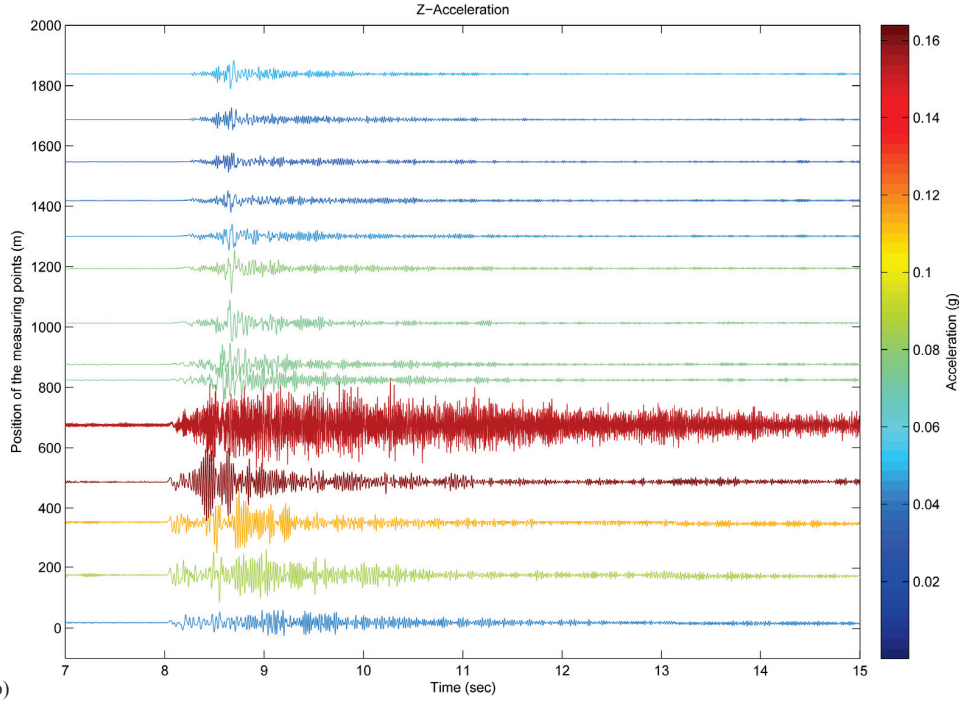

(b)

Fig. 4. Simulation results of (a) horizontal and (b) vertical component acceleration (expressed in $g = 9.81\ m/s^2$) at 14 stations along the ground surface . Note the difference in y-axis scale in (a) and (b).

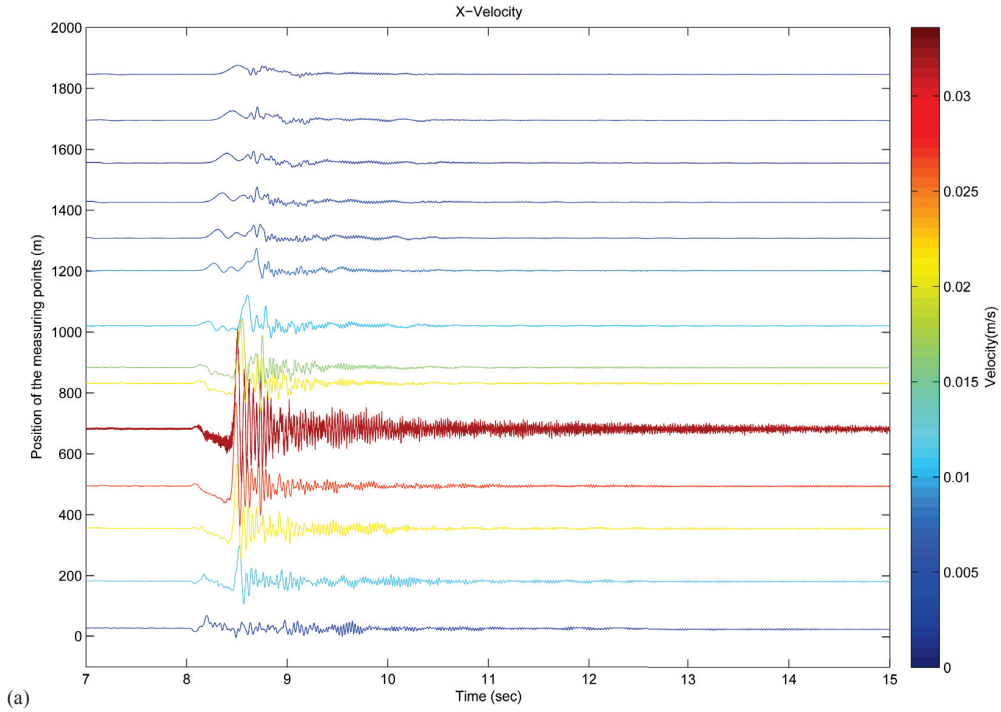

(a)

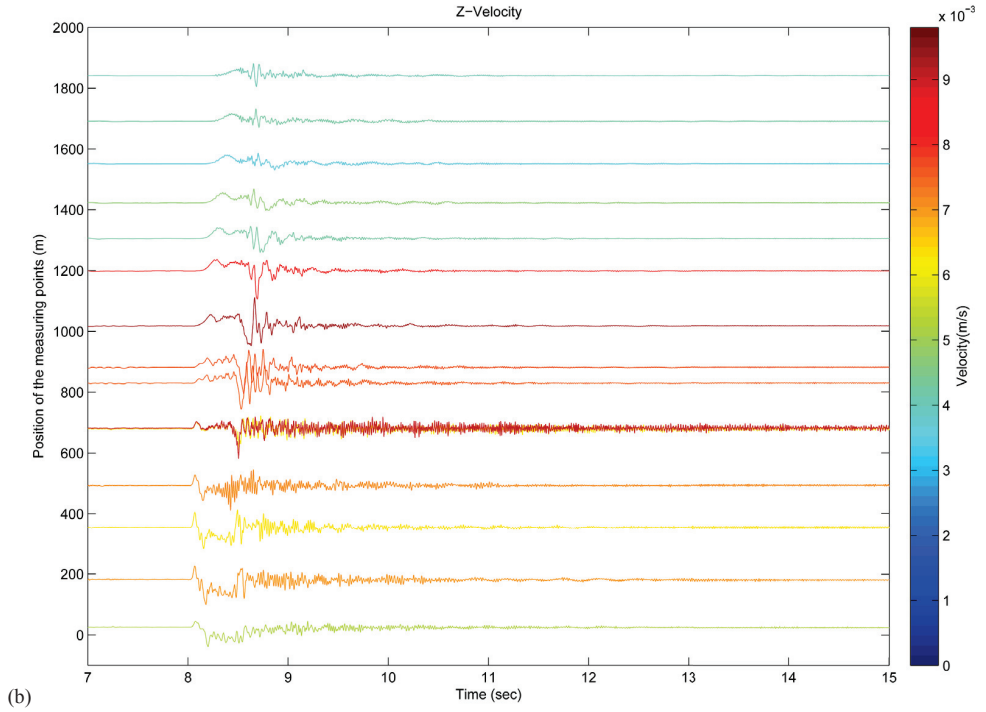

(b)

Fig. 5. Simulation results of (a) horizontal and (b) vertical component velocity at 14 stations along the ground without a softer top soil layer. Note the difference in color scale in (a) and (b).

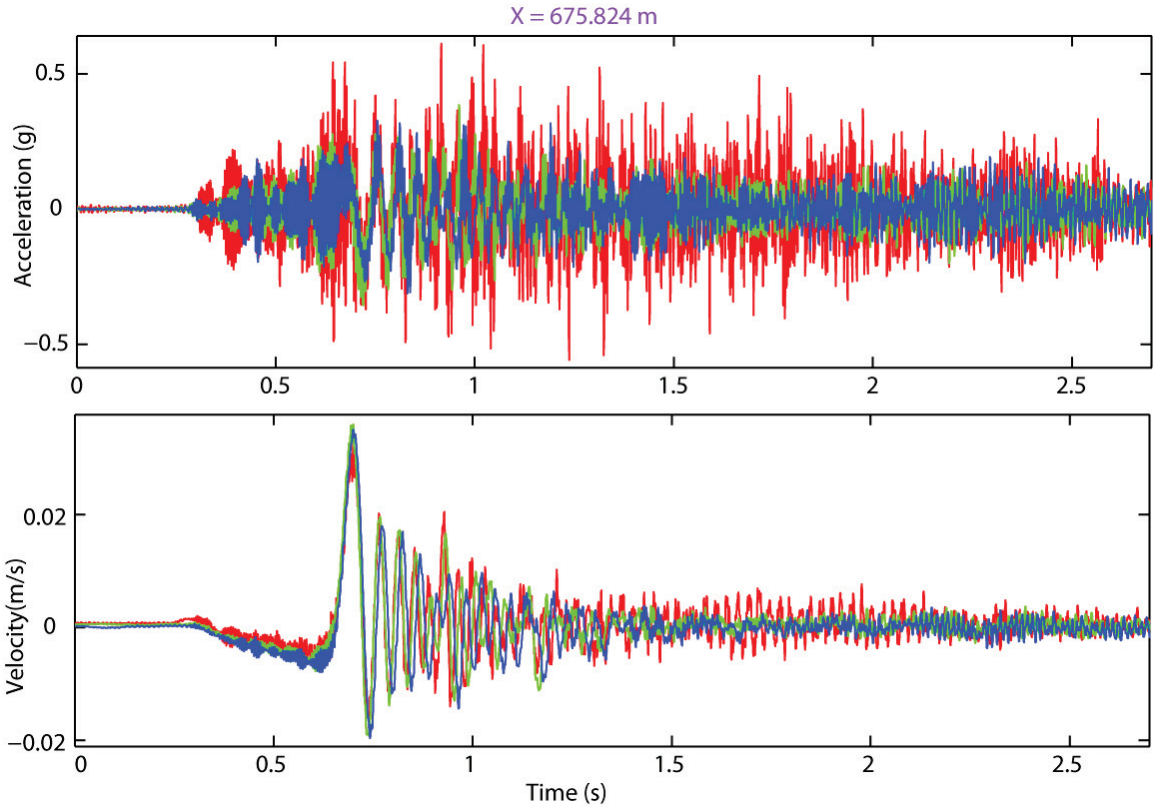

Fig. 6. Close-up view of simulated horizontal (a) acceleration and (b) velocity component at x = 676 m (on top of fault) with and without a softer top soil layer (red = no soil layer, green = 50 m thick soil layer, and blue = 100 m thick soil layer) [7].

5. Assessment of potential building damage and human perception

Following suggestions by Majer et al. [29], in their best-practice protocol for induced seismicity associated with Enhanced Geothermal System (EGS) activities, we considered damage criteria developed for blasting and construction activities. The seismic energy, frequency bandwidth, and range of events generated from these activities are similar to that from shallow injection-induced seismic events. Thresholds for human disturbance and for damage on vulnerable houses are defined in terms of PGV and are almost universally used by the construction and mining industry to assess the potential for threshold cracking due to blasting, and are also employed in many commercially available vibration-monitoring systems [30]. For building damage criteria associated with blasting and mining activities, the "Z-curve or Siskind curve" is the information most often cited. It was published by Siskind et al. [31] as a result of an extensive study conducted in the late 1970s using data from numerous blasts, gathered from monitoring for different types of structures.

Fig. 7 shows the comparison of the PGV and frequency values recorded on the ground surface and the Siskind curve for building damage together with curves for human perception. Curves for building damage in Fig. 7 shows the limits in peak particle velocity (PPV) in inch per second (ips), recommended by the U.S. Bureau of Mines (USBM) to preclude cosmetic damage to plaster and drywall, i.e., the most fragile building materials. As the frequency of the ground motion changes from low to high (1 to 40 Hz) the structure responds less and the limits increase. The limits human perceptions are those specified, as proposed guidelines in the U.S. Army Engineering

Manual EM 1110-2-3800 [32], though originate from studies of human exposure to steady-state sinusoidal vibrations, i.e., not short-duration events.

In Fig. 7 we show an overlay a frequency spectrum processed from velocity record shown in Fig. 6b [7]. We see that the simulated velocity of around 25 mm/s over a frequency of 6 to 15 Hz (green line in Fig. 7) is just above the blue Siskind curve and could therefore potentially cause cosmetic damage (e.g., hairline fracture in drywall or plaster). Moreover, the simulated velocity is above the red line for unpleasant steady-state vibration, which implies that this short duration event would be clearly perceptible by humans.

In Fig. 7 we also inserted single peak velocity and frequency values at different stations along the ground surface. For locations within a few hundred meters from the fault, the peak velocity is around 20 to 30 mm/s at a frequency of about 10 Hz. At larger distances the peak velocity and frequency decreases and stabilizes at about 2.5 mm/s and 2.5 Hz for stations at distances from the fault exceeding 1 km (x = 1500 – 2000 m). According to Fig. 7, a PGV of 2.5 mm/s at 2.5 Hz might be barely perceptible by humans.

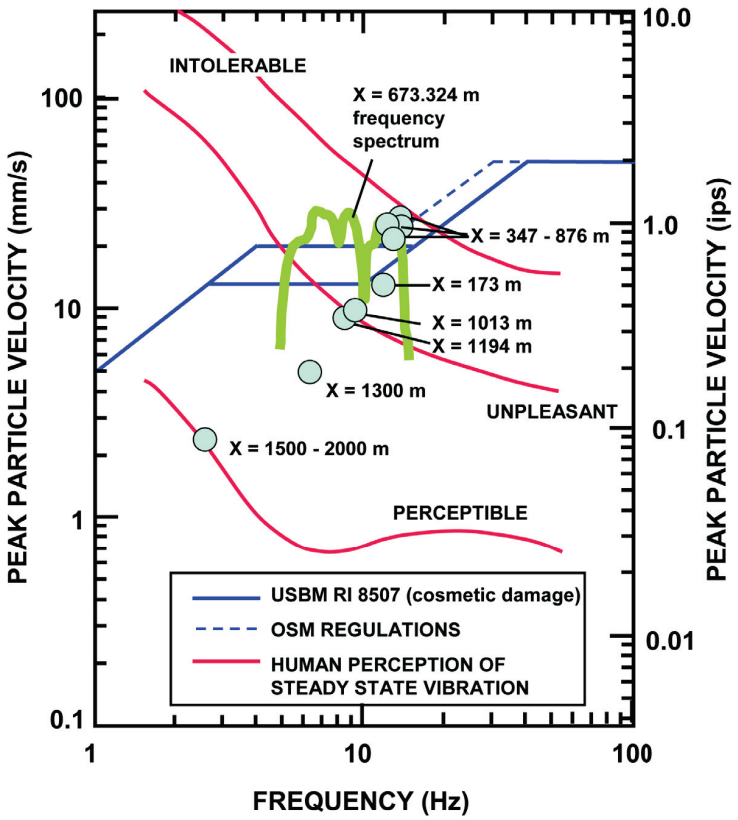

Fig. 7. Comparison of simulated PGV and frequency at different stations to the USBM-recommended limits [27] for cosmetic damage in plaster stucco and drywall and human-perception [28] limits for blast vibration [7]. The frequency spectrum at x = 673.324 is located where the fault intersects the ground surface.

6. Concluding remarks

In addition to comparing our ground motion results to the USMB criterion in Fig. 6, we also compared our simulated PGA and PGV values against the USGS' empirically correlated instrumental intensity scale [33, 34]. If considering the PGA value of 0.6g, we found that the USGS' scale would substantially overestimate the potential damage and human perception, whereas USGS' empirical PGV values are more consistent with the USBM damage criterion. As noted in Rutqvist et al. [7], the reason for overestimating the damage when using USGS' PGA scale is probably that the USGS' empirical correlation was developed based upon eight larger California earthquakes of M $\geqslant$ 5.8 [29, 30] that were tectonic events, which occur much deeper than shallow injection-induced seismic events. Thus, our results confirm the appropriateness of using PGV (rather than PGA) and frequency for the evaluation of potential ground-vibration effects on structures and humans from shallow injection-induced seismic events. Using the USBM criterion, our analysis showed that the short duration, high frequency ground motion generated from the 1000 m deep M_w 3 event may not cause any significant damage to surface structures, but would certainly be felt by the local population.

We note that the seismic event calculated in our synthetic case would not cause any loss of caprock integrity or upward CO_2 leakage toward the ground surface as the fault reactivation took place below injection zone and not through the overlying caprock. This is in line with recent simulation results in Rinaldi et al., [16], who found poor correlation between the seismic events and CO_2 leakage, as relatively small-magnitude (between M_w 2 and 3.5) events are not sufficient to substantially change the permeability along the entire fault length.

We conclude that the likelihood for induced seismicity and leakage will be site specific and a quantitative dynamic model analysis like the one demonstrated in this study could be applied to a real site, for example to study potential consequence of reactivating an identified critical fault, including potential induced seismicity, ground motion, leakage, and effects on surface structures.

Acknowledgments

This work was supported by the Assistant Secretary for Fossil Energy, Office of Natural Gas and Petroleum Technology, through the National Energy Technology Laboratory, under the U.S. Department of Energy Contract No. DE-AC02-05CH11231.

References

[1] Rutqvist J, Tsang C-F. A study of caprock hydromechanical changes associated with CO2 injection into a brine aquifer. Environ Geol 2002; 42:296–305.
[2] Streit JE, Hillis RR. Estimating fault stability and sustainable fluid pressures for underground storage of CO2 in porous rock. Energy 2004; 29:1445–1456.
[3] Hawkes CD, McLellan PJ, Bachu S. Geomechanical factors affecting geological storage of CO2 in depleted oil and gas reservoirs. J Can Pet Technol 2005; 44:52–61.
[4] National Research Council. Induced seismicity potential in energy technologies, National Academies Press, Washington D.C., 2012; pp. 300.
[5] Zoback MD, Gorelick SM. Earthquake triggering and large-scale geologic storage of carbon dioxide. Proc. National Academy of Sciences 2012; doi:10.1073/pnas.1202473109.
[6] Rutqvist J. The geomechanics of CO2 storage in deep sedimentary formations. Geotech Geol Eng 2012; 30:525–551.
[7] Rutqvist J, Cappa F, Rinaldi AP, Godano M. Modeling of induced seismicity and ground vibrations associated with geologic CO2 storage, and assessing their effects on surface structures and human perception. International Journal of Greenhouse Gas Control 2014; 24, 64–77.
[8] Rutqvist J. Status of the TOUGH-FLAC simulator and recent applications related to coupled fluid flow and crustal deformations. Comput Geosci 2011;37:739–750.
[9] Rutqvist J, Birkholzer J, Cappa F, Tsang C-F. Estimating maximum sustainable injection pressure during geological sequestration of CO2 using coupled fluid flow and geomechanical fault-slip analysis. Energy Convers Manage 2007; 48:1798–1807
[10] Cappa F, Rutqvist J, Yamamoto K. Modeling crustal deformation and rupture processes related to upwelling of deep CO2-rich fluids during the 1965–1967 Matsushiro earthquake swarm in Japan. J.Geophys Res 2009; 114:B10304.
[11] Cappa F, Rutqvist J. Modeling of coupled deformation and permeability evolution during fault reactivation induced by deep underground injection of CO2. Int. J. Greenhouse Gas Control 2011; 5:336–346.
[12] Cappa F, Rutqvist J. Impact of CO2 geological sequestration on the nucleation of earthquakes. Geophys. Res. Lett. 2011: 38, L17313.
[13] Mazzoldi A, Rinaldi AP, Borgia A, Rutqvist J. Induced seismicity within geologic carbon sequestration projects: Maximum earthquake magnitude and leakage potential. International Journal of Greenhouse Gas Control 2012;10: 434–442.
[14] Cappa F, Rutqvist J. Seismic rupture and ground accelerations induced by CO2 injection in the shallow crust. Geophysical Journal International 2012;190:1784–1789.
[15] Rinaldi AP, Rutqvist J. Modeling of deep fracture zone opening and transient ground surface uplift at KB-502 CO2 injection well, In Salah, Algeria. International Journal of Greenhouse Gas Control 2013; 12: 155–167.

[16] Rinaldi A.P, Rutqvist J, Cappa F. Geomechanical effects on CO2 leakage through fault zones during large-scale underground injection. Int J Greenhouse Gas Control 2014; 20, 171–131.
[17] Rinaldi AP, Jeanne P, Rutqvist J, Cappa F, Guglielmi Y. Effects of fault-zone architecture on earthquake magnitude and gas leakage related to CO2 injection in a multilayered sedimentary system. Greenhouse Gases: Science and Technology 2014; 4, 99-120.
[18] Konstantinovskaya E, Rutqvist J, Malo M. CO2 storage and potential fault instability in the St. Lawrence Lowlands sedimentary basin (Quebec, Canada): Insights from coupled reservoir-geomechanical modeling. International Journal of Greenhouse Gas Control 2014; 22, 88–110.
[19] Jeanne P., Guglielmi Y., Cappa F., Rinaldi A.P., Rutqvist J. The effects of lateral property variations on fault-zone reactivation by fluid pressurization: application to CO2 pressurization effects within major and undetected fault zones. Journal of Structural Geology, 2014; 62: 97-108.
[20] Pruess, K, Oldenburg C, Moridis G. TOUGH2 User's Guide, Version 2.1, LBNL-43134(revised), Lawrence Berkeley National Laboratory, Berkeley, California 2011.
[21] Itasca. FLAC3D V5.0, Fast Lagrangian Analysis of Continua in 3 Dimensions, User's Guide. Itasca Consulting Group, Minneapolis, Minnesota 2011.
[22] Hanks TC, Kanamori H. A moment magnitude scale. Journal of Geophysical Research 1979; 84: 2348–2350.
[23] Kanamori H, Anderson DL. Theoretical basis of some empirical relations in seismology. Bull Seism Soc Am 1975; 65:1073–1095.
[24] Van Eck T, Goutbeek F, Haak H, Dost B. Seismic hazard due to small-magnitude, shallow-source, induced earthquakes in The Netherlands. Engineering Geology 2006; 87: 105–121.
[25] Bommer JJ, Oates S, Cepeda JM, Lindholm C, Bird J, Torres R, Marroquín G, Rivas J. Control of hazard due to seismicity induced by a hot fractured rock geothermal project. Engineering Geology 2006; 83: 287– 306.
[26] Sharma N, Convertito V, Maercklin N, Zollo A. Ground-motion prediction equations for the Geysers geothermal area based on induced seismicity records. Bulletin of the Seismological Society of America 2013; 103: 117–130.
[27] Wu Y-M, Teng T-L, Shin T-C, Hsiao N-C. Relationship between Peak Ground Acceleration, Peak Ground Velocity, and Intensity in Taiwan. Bulletin of the Seismological Society of America, 2003; 93: 386–396.
[28] Ripperger J, Kästli P, Fäh D, Giardini D. Ground motion and macroseismic intensities of a seismic event related to geothermal reservoir stimulation below the city of Basel—observations and modelling. Geophysical Journal International 2009; 179: 1757–1771.
[29] Majer E, Nelson J, Robertson-Tait A, Savy J, Wong I. Protocol for addressing induced seismicity associated with enhanced geothermal systems. U.S. Department of Energy, January 2012 | DOE/EE-0662, 2012.
[30] Svinkin MR. Minimizing construction vibration effects. Practice Periodical on Structural Design and Construction 2004; 9: 108–115.
[31] Siskind DE, Stagg MS, Kopp JW, Dowding CH. Structure response and damage produced by ground vibrations from surface blasting. Report of Investigations 8507. US Bureau of Mines. Washington, D.C., 1980.
[32] USACE Systematic drilling and blasting for surface excavations. Engineering Manual EM 1110-2-3800US Army Corps of Engineers 1972.
[33] Wald DJ, QuitorianoV, Heaton TH, Kanamori H. Relationships between peak ground acceleration, peak ground velocity and Modified Mercalli Intensity in California. Earthquake Spectra 1999; 15(3): 557–564.
[34] Worden CB, Wald DJ, Rhoades DA. Probabilistic Relationships between Ground-Motion Parameters and Modified Mercalli Intensity in California. Bulletin of the Seismological Society of America 2012; 102: 204 – 221.